Proceedings of the 2006 IASME/WSEAS Int. Conf. on Water Resources, Hydraulics & Hydrology, Chalkida, Greece, May 11-13, 2006 (pp86-91)

# 3D Numerical Simulation of Curved Open Channel Flows

M. De Marchis
University of Palermo
Department of Hydraulic Engineering
and Enviromental Applications
Viale delle Scienze, 90127
ITALY

E. Napoli
University of Palermo
Department of Hydraulic Engineering
and Enviromental Applications
Viale delle Scienze, 90127
ITALY

*Abstract:* Most computational analysis of curved open channel flows conventionally adopt the depth averaged De St. Venant equations. These equations are based on the fundamental assumptions of uniform velocity profile and hydrostatic pressure distribution which doesn't allow to consider secondary flows. In curved open channel flows it is nevertheless very important to study secondary currents. In this memory the results of the simulations in a curved open channel are presented, obtained adopting a fully 3D finite volume numerical discretization to solve the Reynolds Averaged Navier-Stokes equations with the k-$\epsilon$ turbulence model. In order to validate the numerical method, the computed vertical profile of longitudinal and transverse velocities are compared with available experimental data obtained in laboratory. Good agreement is found in the comparisons.

*Key–Words:* Finite-Volume Method, Open Channel Flow, 3D modelling, Channel bends, Velocity distribution

## 1 Introduction

The calculation of flows in curved open channels is an important task in river engineering and related areas. Laboratory experiments to predict the flow field in curved channels are generally very time-consuming, costly and, for many practical applications, very difficult to execute. Their results are nevertheless fundamental to calibrate and validate the numerical models. Until some years ago, the prediction of this kind of flows was mostly made using one dimensional or two dimensional depth-averaged numerical models, based on the conventional De St. Venant equations, that assume uniform velocity and hydrostatic pressure distributions. More recently a number of studies were carried out which assume vertical velocity or pressure distributions to account for the three-dimensionality of the motion. Shimizu et al. [13] assumed a logarithmic vertical distribution of the longitudinal velocity and a hydrostatic pressure distribution to simplify their developed 3D model. The model was tested for an experimental flume having a 180 degree bend. Jin and Steffler [8] developed a 2D depth-averaged numerical model for simulating the velocity distribution in curved open channels. A hydrostatic pressure distribution and parabolic similarity profiles for the longitudinal and transverse velocities were assumed. Lien et al. [10] proposed a 2D depth averaged model for simulating flow patterns in channel bends, which takes into account the influence of the secondary flow through the calculation of the dispersion stresses. Ghamry and Steffler [5] developed a 2D vertically averaged model which resolves the equations of the moment of the momentum too, applying different distribution shapes for velocity and pressure to simulate curved open channel flows.

The influence of the secondary flows, that is one of the dominant features of flows in bends, was nevertheless neglected in these studies. It is however very important to correctly simulate the secondary flows in order to predict the effect of erosion and drift due to the shear stresses at the bottom. For this motive in recent years some attempts have been done to use 3D models to study the flows in bends. In particular Wu et al. [16] developed a 3D numerical model for calculating flow and sediment transport in open channels.

In this paper a 3D numerical model for calculating flows in curved open channels is proposed, that solves the fully 3D Reynolds-Averaged Navier-Stokes equations with the k-$\varepsilon$ turbulence model. To validate the code, the results are compared with experimental data collected in a 270 degree curved rectangular flume [14].

## 2 Governing Equations

The momentum and mass conservation laws (Reynolds Averaged Navier-Stokes and continuity equations) can be written in the conventional summation approach as:

$$\frac{\partial u_i}{\partial t}+\frac{\partial u_i u_j}{\partial x_j}-\nu\frac{\partial^2 u_i}{\partial x_j \partial x_j}+\frac{1}{\rho}\frac{\partial \tau_{ij}}{\partial x_j}+\frac{1}{\rho}\frac{\partial p}{\partial x_i}+g\delta_{i3}=0 \quad (1)$$

$$\frac{\partial u_i}{\partial x_i}=0 \quad (2)$$

where *t* is time, $u_i$ is the *i-th* component of the Reynolds averaged velocity, $x_i$ the *i-th* axis (with the axis $x_3$ vertical and oriented upward), $\rho$ is the water density, *p* is the Reynolds averaged pressure, *g* is the acceleration due to the gravity, $\nu$ is the kinematic viscosity, $\delta_{ij}$ is the Kronecker delta and $\tau_{ij}$ are the Reynolds stresses.

The pressure *p* can be decomposed as the sum of an hydrostatic and a non-hydrostatic part:

$$p=\gamma[(z_B+h)-z]=0 \quad (3)$$

where $z_B$ is the bed elevation from an horizontal plane z=0 of reference, *h* is the water column depth and *q* is the non-hydrostatic pressure.

Introducing equation 3 into equation 1, the Reynolds Averaged Navier-Stokes equations can be rewritten as:

$$\frac{\partial u_i}{\partial t}+\frac{\partial u_i u_j}{\partial x_j}-\nu\frac{\partial^2 u_i}{\partial x_j \partial x_j}+\frac{1}{\rho}\frac{\partial \tau_{ij}}{\partial x_j}+ +\frac{1}{\rho}\frac{\partial q}{\partial x_i}+g\frac{\partial (z_B+h)}{\partial x_i}=0 \quad (4)$$

The turbulent stresses $\tau_{ij}$ are calculated using the *k* - $\varepsilon$ turbulence model in the 'standard' formulation [9], which is based on the eddy viscosity type relation

$$\tau_{ij}=-\rho\nu_t\left(\frac{\partial u_i}{\partial x_j}+\frac{\partial u_j}{\partial x_i}\right)+\frac{2}{3}\delta_{ij}k \quad (5)$$

with

$$\nu_t=c_\mu k^2/\varepsilon \quad (6)$$

where *k* is the turbulent kinetic energy, $\nu_t$ is the eddy viscosity and $\varepsilon$ is the dissipation rate of the turbulent kinetic energy. The turbulent kinetic energy and the dissipation rate are obtained from the following equations:

$$\frac{\partial k}{\partial t}+\frac{\partial u_i k}{\partial x_j}=\frac{\partial}{\partial x_j}\left(\frac{\nu_t}{\sigma_k}\frac{\partial k}{\partial x_j}\right)+P-\varepsilon \quad (7)$$

$$\frac{\partial \varepsilon}{\partial t}+\frac{\partial u_i \varepsilon}{\partial x_j}=\frac{\partial}{\partial x_j}\left(\frac{\nu_t}{\sigma_\varepsilon}\frac{\partial \varepsilon}{\partial x_j}\right)+(c_{\varepsilon 1}P-c_{\varepsilon 2}\varepsilon)\frac{\varepsilon}{k} \quad (8)$$

where P is the production of the turbulent kinetic energy given by:

$$P=\nu_t\left[\frac{\partial u_i}{\partial x_j}+\frac{\partial u_j}{\partial x_i}\right]\frac{\partial u_i}{\partial x_j} \quad (9)$$

The standard values of the model coefficients are used: $c_\mu$=0.09, $c_{\varepsilon 1}$=1.44, $c_{\varepsilon 2}$=1.92, $\sigma_k$=1.0 and $\sigma_\varepsilon$=1.3. The free surface movements are calculated according to the kinematic condition:

$$\frac{\partial h}{\partial t}+u_1\frac{\partial (h+z_B)}{\partial x_1}+u_2\frac{\partial (h+z_B)}{\partial x_2}-u_3=0 \quad (10)$$

The equation 10 together with equation 4 allows to calculate the free surface position at each time step. These equations develop a complete hydrodinamic model able to represent flow fields with mobile boundaries.

# 3 Numerical Application and Comparison with Experimental Results

The simulations were performed using an in-house finite-volume code second order accurate both in time and space. An implicit discretization of vertical turbulent and diffusive terms was employed using the Crank-Nicolson scheme, while the other terms were treated explicitly using an Adam-Bashfort method. A fractional-step method was used for the time advancement, and the free surface elevation was recalculated at each time step according to equation 10. Details on the numerical discretization can be found in Cioffi et al. [3] and Lipari and Napoli [11]. To solve numerically the equations presented in the previous section, boundary conditions are required at each computational boundary. At the lateral walls and the bottom a logarithmic wall-law was used, while at the free surface, in the absence of wind shear, the net fluxes across the surface were set to zero. As inflow conditions, both the velocity and the water surface elevation were imposed, whereas null normal derivatives were imposed at the outflow for all dependent variables. The inflow conditions were obtained from a previous simulation performed in a straight channel using periodic boundary conditions in the streamwise direction. The results of the simulation were compared, to validate the code, with the experimental data obtained by Steffler [14] in a curved open channel. The experiment was conducted at the hydraulic Laboratory of the University of Alberta in Edmonton in a 270 degrees curved open channel. The shape of the cross-section of the channel was rectangular with width 1.07 m and height 0.21 m. The radius of curvature to centerline of the section was 3.66 m. The slope of the bed was

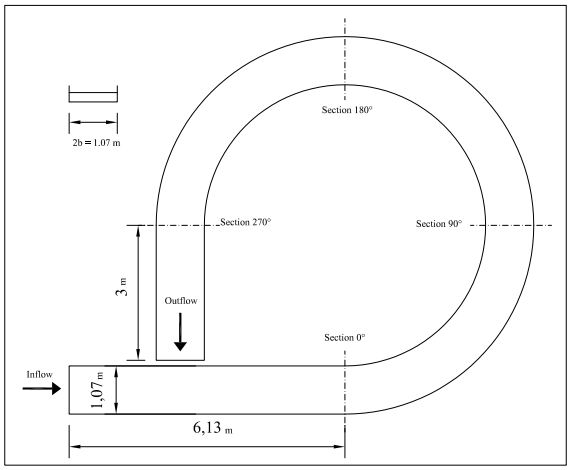


Figure 1: Layout of numerical simulation domain reporting the cross-section of interest.

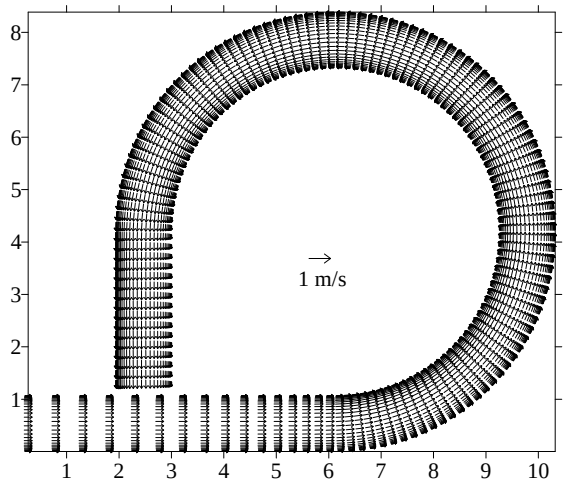


Figure 2: Velocity field averaged along the vertical axis. Distances in meters.

kept constant at the value 0.00083 and the roughness height was estimated to be $k_s$ = 0.0013 m. In the first cross-section of the channel a constant total discharge equal to 0.0235 $m^3$/s was imposed. In figure 1 the laboratory channel used by Steffler, that is composed by a straight part of 6.13 m (inlet), a curvilinear part of 270 degrees and finally another straight part of 3 m (outlet), is plotted.

The simulations were performed in the same domain of the Steffler experiment. The calcolous grid was designed to be fine enough to meet the requirement of reasonable accuracy as well as execution time. The channel was subdivided into 128 x 32 x 16 computational cells in the streamwise (*x*), spanwise (*y*) and vertical (*z*) directions respectively. A non uniform grid was applied in the streamwise and spanwise directions, while a uniform one was adopted along the vertical axis, a refinement was adopted near the bottom. The experimental and numerical longitudinal and transverse velocity profiles over the vertical direction are compared in the following. For comparison the profiles along the vertical direction were normalized by the flow depth. The comparisons were made in the cross-sections corresponding to 0, 90, 180 and 270 degrees (see figure 1). Along each cross-section five profiles were analyzed: two profiles, corresponding to y/b = -0.8 and y/b = 0.8 (where b is half width of the channel and y is the distance from the section centerline, directed toward the internal wall) near the walls, one in the center of the cross-section (y/b=0) and finally two profiles, corresponding to y/b = -0.4 and y/b = 0.4, away from the walls. In figure 1 the cross-sections of interest are also reported.

In figure 2 the depth averaged velocity field is plotted. In the straight part the velocity profile over the cross-section is obviously symmetric, while in the curved part and at the outflow the velocities are clearly larger near the external wall.

In figure 3, the experimental and numerical predicted longitudinal velocity profiles over the vertical direction are compared. The comparison clearly shows that the agreement of the longitudinal velocity profile is very satisfactory in all cross-sections of comparison.

In figure 4 the transverse velocity profile are compared. The numerical and experimental results are in very good agreement principally in the cross-section of the curved part corresponding to 270 degrees, whereas in the others sections the same inversion point was found but the speed of the secondary currents was underestimated by the numerical model. In order to investigated the reason of this underestimation new simulations were performed using a more refined grid in the vertical direction. Since no significant differences were founded, the different recirculation effect is probably due to the insufficient refinement of the grid in the streamwise direction and to the null derivative boundary conditions imposed at the outflow section, which is not sufficiently far away from the end of the curved part.

The recirculation effect shown in figure 4 can be better analized plotting the velocities in some transverse cross-sections. In particular in figure 5 the velocity fields in the cross-sections corresponding to 90, 180 and 270 degrees are plotted. All cross sections are occupied by a large recirculation region; in the sections at 90 and 180 degrees a net mass flux is observed towards the internal wall, which is counterbalanced, to ensure the mass conservation, by an acceleration in the streamwise direction near the same wall.

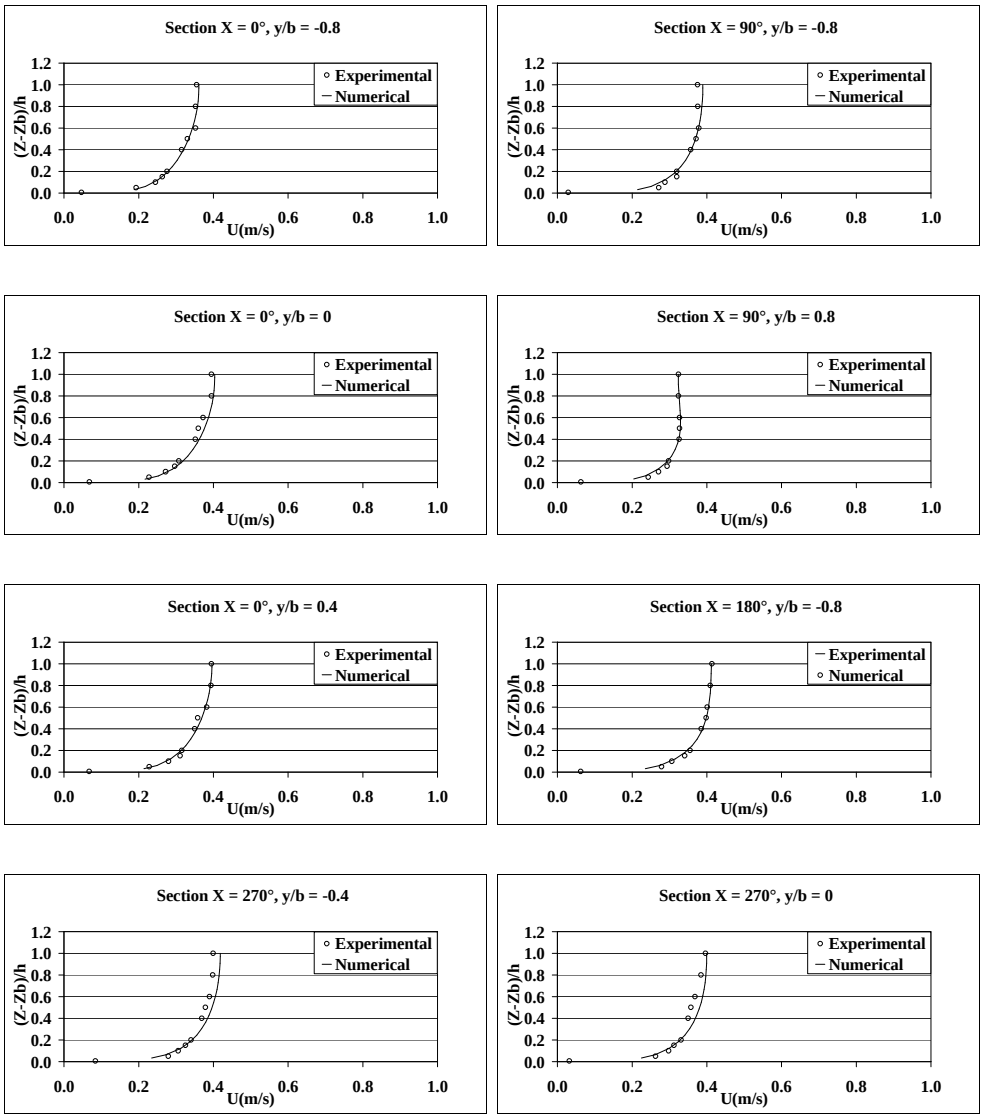


Figure 3: Comparison of longitudinal velocity profiles for Steffler's experiments (1984).

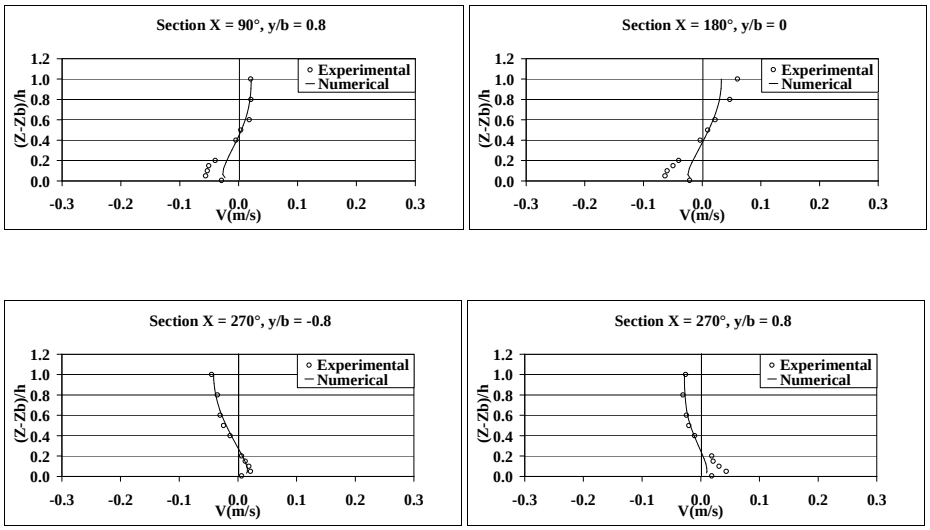


Figure 4: Comparison of transverse velocity profiles for Steffler's experiments (1984).

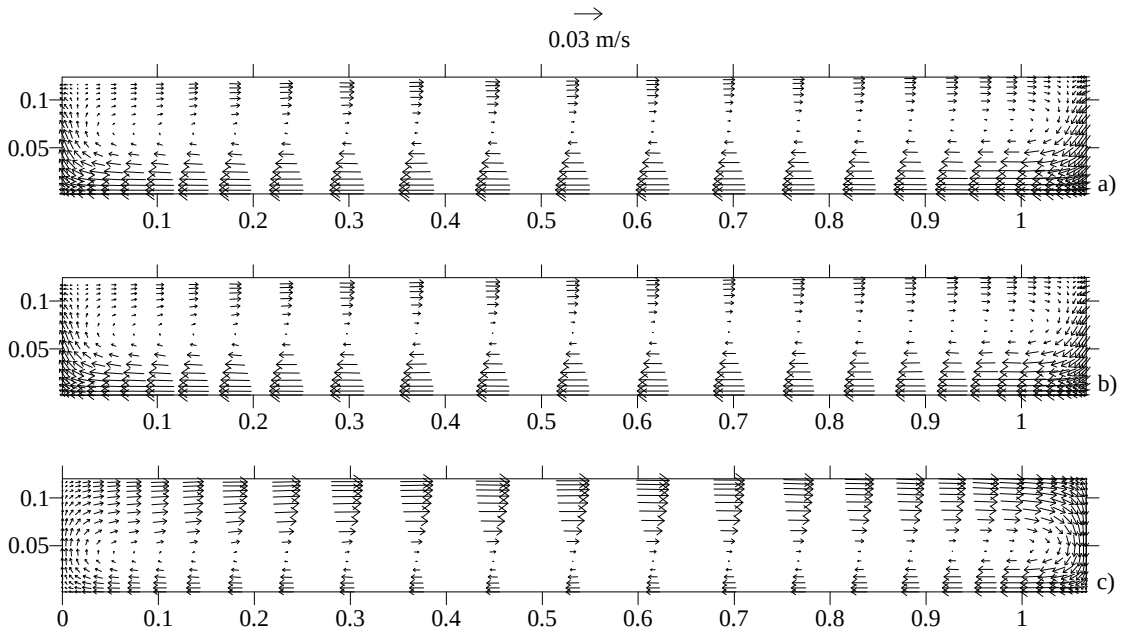


Figure 5: Transverse velocity fields in the cross-sections a) 90 b) 180 c) 270 degrees. Vertical scale distorted, distances in meters.

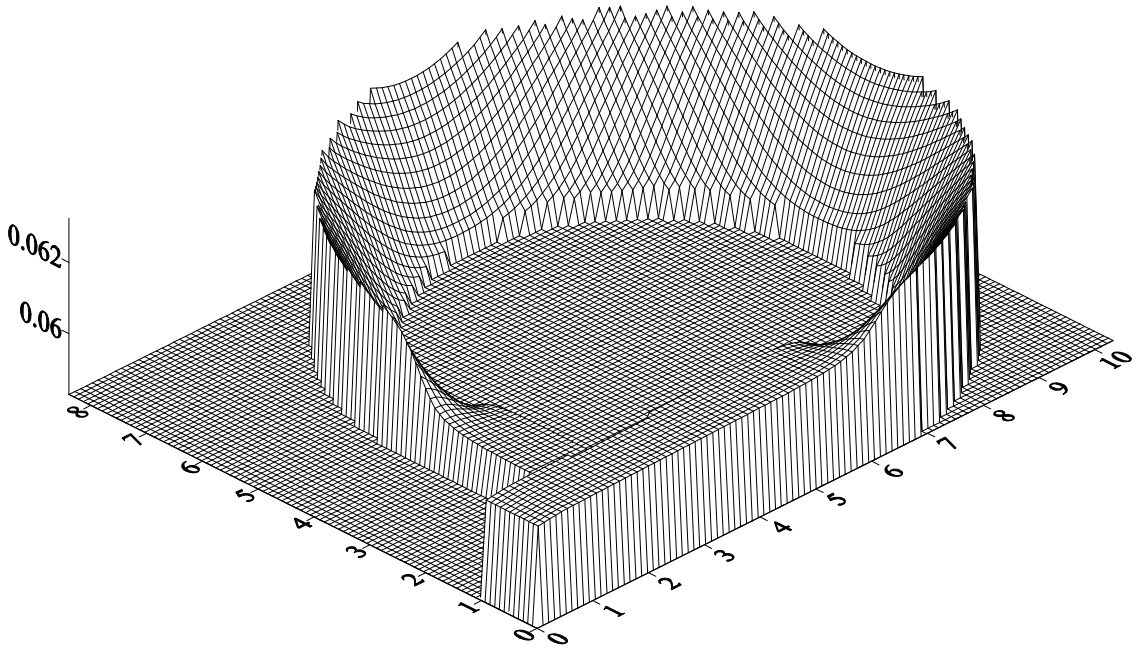


Figure 6: Free surface elevation.

In the cross-section at 270 degrees, that is the last section of the curved part of the channel, an acceleration in the streamwise direction is on the contrary observed near the external wall, which is in accordance with the net flux of mass towards th external wall, which can be seen in figure 5c.

In figure 6 finally the position of the free surface in the steady state is plotted. The rotation of the free surface is clearly seen, with an elevation at the external wall and a lowering near the internal wall. The pressure gradients due to the free-surface elevations are thus responsable for the secondary flows directed inward, while inertial effects cause the outward secondary flows showed in figure 6.

# 4 Conclusions

A fully 3D numerical model has been used to simulate the flow field in a curved open channel composed by an inflow straight part, a curvilinear one with a bend of 270 degrees and finally an outflow straight part.

In order to validate the numerical model proposed, the results of the numerical simulation has been compared with the experimental data collected in a 270 curved rectangular flume by Steffler[14]. The comparison with the experimental results showed that the numerical model is able to correctly predict the behaviour of the flow field. In particularly an excellent agreement between numerical and experimental longitudinal velocity profiles along the vertical direction was found in all cross-section of interest. Little differences were found in the comparison of the transverse velocity profiles with a light underestimation of the recirculation effect at the bottom and near the free surface, even if the inversion point was correctly simulated. These defferences are probabily due to the insufficient grid refinement in the streamwise direction. The effect of the rotation of the free surface due to the bend was correctly obtained with the elevation at the external wall and the lowering near the internal one. This is in accord with the transverse velocity fields shown.

*References:*


[1] K. Blanckaert and W.H. Graf, Momentum transport in Sharp Open-Channel Bends, *J. Hydraul. Eng.*, 130(3), 2004, pp. 186-198.

[2] K. Blanckaert and H.J. de Vriend, Secondary Flow in Sharp Open-Channel Bends, *J. Fluid Mech.*, 498, 2004, pp. 353-380.

[3] F. Cioffi, F. Gallerano and E. Napoli, Three-dimensional numerical simulation of wind-driven flows in closed channels and basins. *J. Hydraul. Res.*,43(3), 2004, pp. 290–301.

[4] H. Ghamry and P. Steffler, Effect of applying different distribution shapes for velocities and pressure on simulation of curved open channel, *J. Hydraul. Eng.*, 128(11), 2002, pp. 969-982.

[5] J.G. Duan, Simulation of Flow and Mass Dispersion in Meandring Channels, *J. Hydraul. Eng.*, 130(10), 2004, pp. 964-976.

[6] H.K. Ghamry and P.M. Steffler, Two Dimensional Vertically Averaged and Moment Equations for Rapidly Varied Fows, *J. Hydraul. Res.*, 40(5), 2004, pp. 579–587.

[7] Q.C. Guo and Y.C. Jin, Modeling Sediment Transport Using Depth-Averaged and Moment Equations, *J. Hydraul. Eng.*, 125(12), 1999, pp. 1262–1269.

[8] Y. Jin and P. Steffler, Depth-averged and moment equations for moderately shallow free surface flow, *J. Hydraul. Res.* 31(1), 1993, pp. 5-17.

[9] B.E. Launder and D.B. Spalding, The numerical computation of turbulent flows, *Comp. Meth. Appl. Mech. Eng.*, 3, 1974.

[10] H. Lien, T. Hsieh, J. Yang, and K. Yeh, Bend-Flow Simulation Using 2D Depth-Averaged Model, *J. Hydraul. Eng.*, 125(10), 1999, pp. 1097-1108.

[11] G. Lipari and E. Napoli, The impacts of the ALE and hydrostatic-pressure approaches on the energy budget of unsteady free-surface flows, *Computer and Fluids*, submitted 2006.

[12] T. Molls and H. Chaudhry, Depth Averaged Open Channel Flow Model, *J. Hydraul. Eng.* 121(6), 1995, pp. 453–465.

[13] Y. Shimizu, H. Yamaguchi and T. Itakura, Three-dimensional computation of flow and bed deformation, *J. Hydraul. Eng.* 116(9), 1990, pp. 1090–1108.

[14] P. Steffler, *Turbulent flow in curved rectangular channel*, Univ. of Alberta, Canada, PhD thesis, 1984.

[15] J. Ye and J.A. McCorquodale, Depth-Averaged Open-Channel Flow Model, *J. Hydraul. Res.*, 121(6), 1995, pp. 453–465.

[16] W. Wu, W. Rodi, and T. Wenka, 3d numerical modelling of flow and sediment transport in open channel, *J. Hydraul. Eng.*, 126(1), 2000, pp. 4-15.

[17] J. Ye and J.A. McCorquodale, Depth-Avegaged Hydrodynamic Model in Curvilinear Collocated Grid, *J. Hydraul. Res.*, 123(5), 1997, pp. 380–388.